Clinical Science (2020) **134** 941–953
https://doi.org/10.1042/CS20200065

PORTLAND PRESS

Research Article

An inducible intestinal epithelial cell-specific NHE3 knockout mouse model mimicking congenital sodium diarrhea

Jianxiang Xue[1], Linto Thomas[1], Maryam Tahmasbi[2], Alexandria Valdez[1], Jessica A. Dominguez Rieg[1], Robert A. Fenton[3] and Timo Rieg[1]

[1]Department of Molecular Pharmacology and Physiology, University of South Florida, Tampa, Florida; [2]Department of Pathology and Cell Biology, University of South Florida, Tampa, Florida; [3]Department of Biomedicine, Aarhus University, Aarhus, Denmark

Correspondence: Timo Rieg (trieg@usf.edu)

The sodium–hydrogen exchanger isoform 3 (NHE3, *SLC9A3*) is abundantly expressed in the gastrointestinal tract and is proposed to play essential roles in Na^+ and fluid absorption as well as acid–base homeostasis. Mutations in the *SLC9A3* gene can cause congenital sodium diarrhea (CSD). However, understanding the precise role of intestinal NHE3 has been severely hampered due to the lack of a suitable animal model. To navigate this problem and better understand the role of intestinal NHE3, we generated a tamoxifen-inducible intestinal epithelial cell-specific NHE3 knockout mouse model ($NHE3^{IEC\text{-}KO}$). Before tamoxifen administration, the phenotype and blood parameters of $NHE3^{IEC\text{-}KO}$ were unremarkable compared with control mice. After tamoxifen administration, $NHE3^{IEC\text{-}KO}$ mice have undetectable levels of NHE3 in the intestine. $NHE3^{IEC\text{-}KO}$ mice develop watery, alkaline diarrhea in combination with a swollen small intestine, cecum and colon. The persistent diarrhea results in higher fluid intake. After 3 weeks, $NHE3^{IEC\text{-}KO}$ mice show a ∼25% mortality rate. The contribution of intestinal NHE3 to acid–base and Na^+ homeostasis under normal conditions becomes evident in $NHE3^{IEC\text{-}KO}$ mice that have metabolic acidosis, lower blood bicarbonate levels, hyponatremia and hyperkalemia associated with drastically elevated plasma aldosterone levels. These results demonstrate that intestinal NHE3 has a significant contribution to acid–base, Na^+ and volume homeostasis, and lack of intestinal NHE3 has consequences on intestinal structural integrity. This mouse model mimics and explains the phenotype of individuals with CSD carrying *SLC9A3* mutations.

Introduction

Sodium (Na^+) absorption is accomplished by several different processes. Postprandial, secondary active transport processes including Na^+/glucose cotransport and Na^+/amino acid cotransport both significantly contribute to intestinal Na^+ absorption. In addition, Na^+/H^+ exchange, in particular via the Na^+/H^+ exchanger isoform 3 (NHE3), is a critical mechanism for transepithelial movement of Na^+, HCO_3^- and water in the basal and postprandial state [1,2]. In the mouse, NHE3 is highly expressed in all small intestinal segments (jejunum > duodenum > ileum) and the colon [3,4]. Functionally, luminal NHE3 is coupled to Cl^-/HCO_3^- exchange (DRA, down-regulated in adenoma) [5] or H^+/amino acid cotransport (PAT1, putative anion transporter 1) [6] that mediates electroneutral NaCl absorption. Genetic global deletion of NHE3 in mice ($NHE3^{-/-}$) causes diverse problems associated with NHE3 function in the intestine and the kidney [7,8]. $NHE3^{-/-}$ mice suffer from mild diarrhea, mild metabolic acidosis, dilation of the intestinal tract and a high mortality rate subsequent to weaning, with only ∼30% of mice surviving into adulthood [9]. When fed a low NaCl diet, $NHE3^{-/-}$ mice experience severe dehydration resulting in

Received: 14 January 2020
Revised: 25 March 2020
Accepted: 27 March 2020

Accepted Manuscript online: 30 March 2020
Version of Record published: 21 April 2020

Clinical Science (2020) **134** 941–953
https://doi.org/10.1042/CS20200065

hypovolemia, body weight loss and death [10]. When $NHE3^{-/-}$ mice are fed a high–NaCl diet (5% NaCl), the small intestine becomes severely swollen, consequently resulting in death within 2 days [11]. This is attributed to the osmotic effect exerted by the high NaCl levels in the intestine. Taken together, a high mortality rate, deletion of NHE3 in both intestine and kidney, and prenatal NHE3 deletion leading to potentially confounding developmental problems are significant drawbacks of previously generated NHE3 knockout models.

In 1985, two groups independently described diarrheal disorders that were classified as congenital sodium diarrhea (CSD) [12,13] and ascribed it to defective handling of Na^+ and H^+. The molecular origin remained unknown until Janecke et al. [14] identified recessive missense, splicing and truncation mutations in NHE3 that resulted in reduced basal surface expression and/or loss of basal transport activity when the mutants were overexpressed in NHE-deficient fibroblasts. Overall, ∼50 cases of CSD have been identified [15]. These patients are characterized by intrauterine onset of diarrhea resulting in polyhydramnios, and, after birth, severe dehydration, weight loss, hyponatremia and metabolic acidosis [16]. The electrolyte imbalances in the most severe cases are associated with a high risk of mortality.

Our previous studies indicated that renal NHE3 plays a minor role in acid–base regulation under baseline conditions [3], emphasizing the importance of the intestine. Therefore, in the present study we wanted to categorically determine the role of NHE3 in the intestine to acid–base regulation and test the hypothesis that lack of intestinal NHE3 in adulthood mimics CSD. As conditional non–inducible intestinal epithelial cell–specific NHE3 knockout mice and $NHE3^{-/-}$ mice have high mortality [17], we generated tamoxifen–inducible intestinal epithelial cell–specific NHE3 knockout mice ($NHE3^{IEC\text{-}KO}$) to test our hypothesis. Our results in $NHE3^{IEC\text{-}KO}$ mice demonstrate that intestinal NHE3 significantly contributes to (i) acid–base homeostasis, (ii) Na^+/K^+ homeostasis and (iii) fluid absorption, defects in which cannot be fully compensated for by altered renal function. Cumulatively, the phenotype of $NHE3^{IEC\text{-}KO}$ mice resembles the phenotype of patients with CSD.

Materials and methods

Animals

All animal experiments were conducted in accordance with the Guide for Care and Use of Laboratory Animals (National Institutes of Health, Bethesda, MD) and were approved by the local Institutional Animal Care and Use Committee, USF. All animal experiments were performed at the USF. Mice were housed under a 12:12-h light:dark cycle in standard rodent cages with free access to standard rodent chow (TD.2018, Envigo, Madison, WI) and tap water. Floxed NHE3 ($NHE3^{loxlox}$) female mice [18] were crossed with hemizygous male villin–$CreER^{T2}$ mice (Stock No: 020282, The Jackson Laboratories, Bar Harbor, ME) that express the Cre recombinase transgene specifically in intestinal epithelial cells. From the filial (F) 1 progeny, male mice heterozygous for the floxed NHE3 allele ($NHE3^{lox/wild\text{-}type}$) and villin–$creER^{T2}$ were bred to $NHE3^{loxlox}$ mice to generate final breeder pairs in the F2 progeny. To generate male experimental intestinal epithelial–specific NHE3 knockout ($NHE3^{IEC\text{-}KO}$) mice and control ($NHE3^{loxlox}$) mice, female $NHE3^{loxlox}$ mice were bred to male $NHE3^{IEC\text{-}KO}$ mice. Mice were genotyped by polymerase chain reaction from genomic DNA isolated from ear punch as published previously [3,19]. NHE3 deletion was induced by application of tamoxifen (67 mg/kg), initially dissolved in 5% (v/v) of ethanol followed by adding 95% (v/v) of corn oil. Tamoxifen was administered via oral gavage (volume 1% of body weight) for five consecutive days to control and $NHE3^{IEC\text{-}KO}$ mice.

Physiological analysis

Body weight, fluid and food intake were determined daily [20] before induction, during induction and up to 27 days after induction. One week before induction, plus at the end of the experimental period, blood was collected under brief isoflurane anesthesia from the retro-orbital plexus for analysis. Spontaneous voided urine was collected by reflex urination holding mice over a clean Petri dish [21].

Urine and blood analysis

Blood chemistry was determined by an OPTI® CCA-TS2 blood gas analyzer [3] using an E-Cl Type cassette (OPTI-Medical, Roswell, GA). Urine osmolality was measured using an Osmomat 3000 (Gonotec GmbH, Berlin, Germany). Urinary pH was determined using a pH electrode (9810BN, Fisher Scientific, Pittsburgh, PA). Plasma aldosterone was determined using a solid phase enzyme-linked immunosorbent assay (IBL America, Minneapolis, MN). Blood glucose was determined by a glucose meter (Contour, Bayer, Parsippany, NJ) from blood collected via tail snip.

Intestinal permeability and fecal water content

Mice were gavaged with fluorescein isothiocyanate (FITC) conjugated-dextran (FD–4, molecular weight of 3–5 kDa, Sigma-Aldrich, 22 mg/ml, 1% of body weight) 2 weeks after tamoxifen induction [22]. Blood from a tail snip was collected in 10 μl minicaps® (Hirschmann Laborgeräte, Eberstadt, Germany) at 1, 2 and 4 h after gavage. After centrifugation, samples were diluted 1:10 in 0.5 mol/L HEPES (pH 7.4) and FD–4 concentrations determined using a fluorescent microplate reader (Cytation 3, Biotek, Winooski, VT). Fecal water content in freshly defecated stool was calculated as the difference in fresh weight versus dry weight. Fecal dry weight was measured after 24 h at 80°C when mass was stable [23].

Isolation of intestinal epithelial cells

Freshly isolated epithelial cells were prepared by calcium (Ca^{2+}) chelation [23]. Briefly, the small intestine was removed and flushed with 10 ml ddH_2O, The flushing solution was collected, and the pH determined. The intestine was everted, one end was ligated, and the everted small intestine was filled with Ca^{2+}–free PBS containing 5 mmol/L ethylenediaminetetraacetic acid (EDTA), pH 7.4. The everted pieces were put in 50 ml tubes containing 40 ml Ca^{2+}–free PBS+EDTA and incubated in a water bath at 37°C for 20 min. Every 5 min, the tubes were vigorously shaken to release the epithelial cells. After removal of sacs devoid of epithelial cells, the solution was split in half and the tubes were centrifuged. One pellet was prepared for mRNA analysis the other pellet for Western blotting.

Morphological analysis of the intestine

In another set of mice, the small intestine and colon were collected from each animal and measured in length. In addition, small intestinal weight was determined before flushing with ice-cold PBS. Afterward, tissue was fixed overnight in 4% paraformaldehyde, paraffin embedded, and sectioned at 4–6 μm. After deparaffinization and rehydration, sections were stained with hematoxylin and eosin (H&E) for morphometry. In H&E-stained jejunal sections, villus length and crypt depth were measured in 12–15 well-oriented crypt-villus units per animal using a 40–1000× infinity research laboratory compound microscope with built in camera display. Measurements were performed by the software integrated measurement tools in TouchScope (version 2.5.6; Amscope, Irvine, CA) [24]. For cleaved caspase-3 staining, small intestine and colon sections were incubated in 3% H_2O_2 for 10 min, heated in Antigen Decloaker (Biocare Medical, Concord, CA) for 45 min, blocked with 20% normal goat serum (Vector Laboratories, Burlingame, CA), and then incubated with rabbit polyclonal cleaved caspase-3 antibody (1:100; Cell Signaling Technology, Beverly, MA) for 1 h at room temperature. Sections were then incubated with goat anti-rabbit biotinylated secondary antibody (1:200; Vector Laboratories) for 30 min at room temperature. Vectastain Elite ABC reagent (Vector Laboratories) was then applied, followed by diaminobenzidine as substrate. Sections were counterstained with hematoxylin, dehydrated and mounted with coverslips. Apoptosis in the intestinal epithelium was quantified using the number of cleaved caspase-3-positive cells 100 well–oriented contiguous crypts (jejunum and colon) and 50 well–oriented villi (jejunum) per animal [24]. All counting was performed by an examiner (J.A.D.R) blinded to sample identity.

Analysis of inflammation

H&E-stained small intestine and colon sections were graded by using the following scheme: 0 = normal colonic mucosa with no active inflammation; 1 = mild active inflammation; 2 = moderate active inflammation; 3 = severe active inflammation. The highest score seen in sections was reported for each mouse. All scoring was performed by a pathologist (M.T.) blinded to sample identity.

Immunofluorescent labeling of intestinal and kidney sections

Tissue preparation, sectioning and labeling were performed as previously described [21,23]. Goat anti-rabbit Texas Red conjugated secondary antibody (TI–1000, Vector Laboratories, Burlingame, CA) was used for visualization of NHE3 labeling (SPC–400, StressMarq Biosciences, Cadboro Bay, Victoria, British Columbia, Canada). Sections were mounted using hardset antifade mounting medium with DAPI (H–1500, Vector Laboratories). An Olympus (Center Valley, PA) FV1000 MPE Multiphoton Laser Scanning Microscope with a 40× UPLFL objective lens (numerical aperture: 0.75) was used for imaging of labeled sections.

Reverse-transcription quantitative polymerase chain reaction

Total RNA from freshly isolated intestinal epithelial cells and whole kidney was isolated from control and $NHE3^{IEC\text{-}KO}$ mice and homogenized using a Tissue Tearor (Bartlesville, OK) and QIAshredder (Qiagen, Valencia, CA) according to the manufacturer's instructions. The extracted RNA was further purified using RNeasy Plus Mini Kit (Qiagen).

Clinical Science (2020) **134** 941–953
https://doi.org/10.1042/CS20200065

cDNA was made by reverse transcribing total RNA using a QuantiTect reverse transcription kit (Qiagen) according to the manufacturer's instructions. Quantitative real-time PCR was performed using TaqMan™ Universal PCR Master Mix (Fisher Scientific) in a QuantStudio 3 (Applied Biosystems, Foster City, CA). Template concentration was 12.5 ng reverse-transcribed RNA/25–μl reaction (performed in triplicates) and was used in conjunction with primer pairs specific for NHE3 (Mm01352478_g1, efficiency 98%) and with GAPDH (Mm99999915_g1) as a reference gene. Data analysis used the $\Delta\Delta C_t$ method, i.e. cycle thresholds (C_t), were normalized to GAPDH expression and compared with control [25].

Immunoblot analysis

Renal tissue and acutely isolated intestinal epithelial cells were homogenized in buffer containing protease inhibitor (250 mmol/L sucrose, 10 mmol/L triethanolamine, Sigma-Aldrich, St. Louis, MO; Fisher Scientific, respectively) and phosphatase inhibitor (Fisher Scientific). The homogenate was centrifuged at 1000 ***g*** for 15 min, and the resultant supernatant further centrifuged at 17,000 ***g*** for 30 min. Pellets were resuspended and used for Western blotting. For ZO–1, the supernatant of the 1000 ***g*** spin was used for Western blotting. Equal lane loading (15 μg for kidney and 20 μg for intestine) was achieved using a Bio-Rad DC Protein assay (Bio-Rad Laboratories, Richmond, CA). Samples were resolved on NuPAGE 4–12% Bis-Tris gels in MOPS buffer or NuPAGE 3-8% Tris-Acetate gels (for occludin and ZO-1, Fisher Scientific). Gel proteins were transferred to PVDF membranes and immunoblotted with antibodies against NHE3 (dilution 1:500, rabbit, MilliporeSigma, Burlington, MA), occludin (dilution 1:500, mouse, Invitrogen, Carlsbad, CA), ZO–1 (dilution 1:250, rabbit, Invitrogen) and ß–actin (dilution 1:30,000, mouse, Sigma-Aldrich; dilution 1:5,000, rabbit, Proteintech, Rosemont, IL). Detection was performed with secondary antibodies against rabbit or mouse and detected with an Odyssey® CLx (LI-COR Biosciences, Lincoln, NE). Densitometric analysis was performed by using Image Studio Lite (LI–COR Biosciences).

Statistical analysis

Data are expressed as mean ± S.E.M. Unpaired Student's *t* test or Mann–Whitney *U* test was performed as appropriate to analyze for statistical differences between groups. One-way analysis of variance (ANOVA) or two–way mixed effects ANOVA followed by two–stage linear step–up procedure of Benjamini, Krieger and Yekutieli or Tukey multiple comparison tests as indicated were used to test for significant differences between genotype and experimental conditions. Significance was considered at $P < 0.05$.

Results

Confirmation of NHE3 knockout in intestinal epithelial cells

$NHE3^{IEC\text{-}KO}$ mice were born at predicted Mendelian frequencies, appeared grossly indistinguishable from control mice, and developed normally. At the end of the experimental period (27 days after tamoxifen administration) qualitative immunofluorescence identified NHE3 along the villi of the small intestine in control mice (Figure 1A). In contrast, this labeling was completely absent in $NHE3^{IEC\text{-}KO}$ mice (Figure 1B). Staining intensity and NHE3 localization in the kidney were not different between control and $NHE3^{IEC\text{-}KO}$ mice (Figure 1C,D). NHE3 messenger RNA (mRNA) and protein levels were virtually undetectable in acutely isolated intestinal epithelial cells (Figure 1E,F). Renal NHE3 protein levels were ∼2-fold higher in $NHE3^{IEC\text{-}KO}$ compared with control mice after tamoxifen administration (Figure 1F). Of note, survival analysis identified that 3 weeks after tamoxifen administration $NHE3^{IEC\text{-}KO}$ mice have a ∼25% mortality rate (Figure 1G).

Intestinal analysis of control and $NHE3^{IEC\text{-}KO}$ mice

Fecal samples from $NHE3^{IEC\text{-}KO}$ mice showed visible signs of diarrhea (Figure 2A), with ∼1.45–fold higher fecal water content compared with control mice (Figure 2B). Around 35% of $NHE3^{IEC\text{-}KO}$ mice had visible watery diarrhea. Morphologically, all $NHE3^{IEC\text{-}KO}$ mice had dilated small intestines, cecum and colon (Figure 2C). This was associated with significantly higher intestinal permeability, demonstrated by ∼1.9-fold higher FD–4 plasma concentrations 4 h after administration (Figure 2D). Analysis of tight junction protein expression showed that occludin in the small intestine was decreased by ∼28% in $NHE3^{IEC\text{-}KO}$ compared with control mice (Figure 3A). In contrast, ZO–1 expression was not significantly different between genotypes (Figure 3A). Histologically, no observable difference in inflammation was detected in the small intestine between genotypes. Examination of colon sections (Figure 3B and Supplementary Figure S1) showed that 44% of $NHE3^{IEC\text{-}KO}$ mice had pathological findings: 11% showed patchy cryptitis with occasional crypt abscesses and 33% showed focal/patchy mild cryptitis. Of note, all the control mice and 56% of $NHE3^{IEC\text{-}KO}$ mice had no pathological findings. Cleaved caspase-3 staining, a specific marker for apoptosis, was

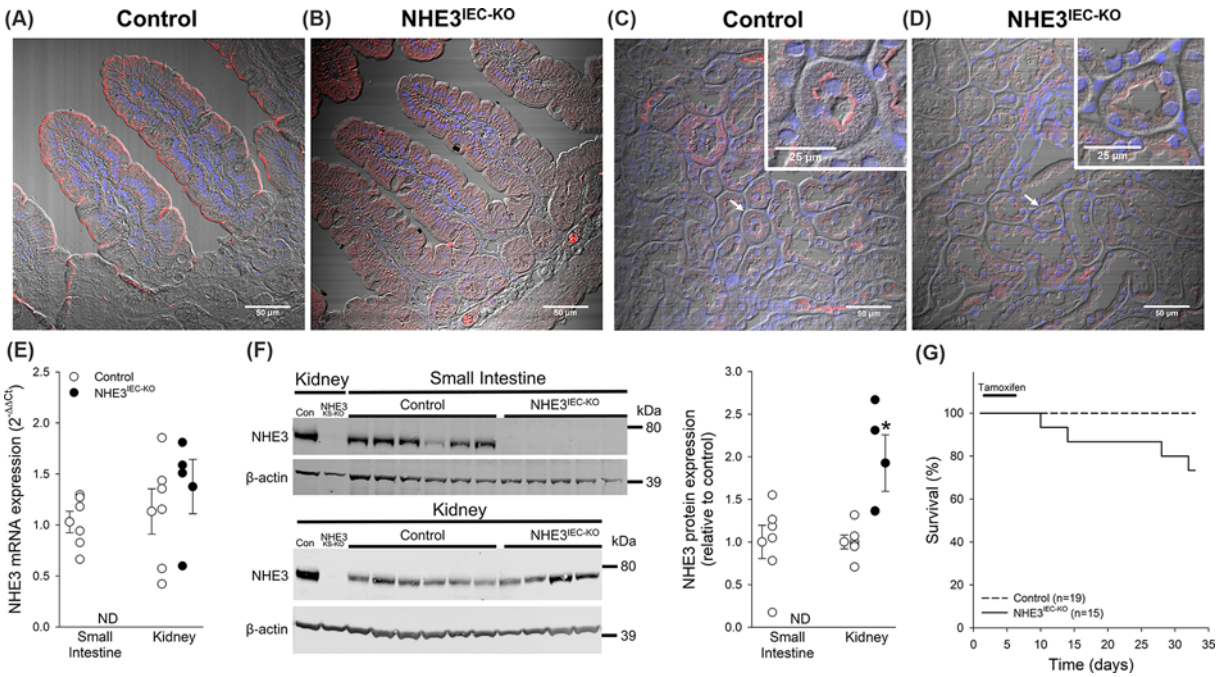

Figure 1. Effect of intestinal epithelial cell-specific NHE3 knockout on mortality and renal NHE3

(**A**) Representative confocal microscopy images of small intestinal and renal NHE3 abundance in tamoxifen treated control and NHE3^{IEC-KO} mice. Control mice show NHE3 immunofluorescent labeling in the apical membrane of enterocytes; in contrast, (**B**) NHE3^{IEC-KO} mice completely lack this immunofluorescent labeling. Labeling of renal NHE3 was not different between (**C**) control and (**D**) NHE3^{IEC-KO} mice. (**E**) mRNA expression of NHE3 in NHE3^{IEC-KO} mice was not detectable (ND) in acutely isolated intestinal epithelial cells. No differences were observed in renal NHE3 mRNA expression. (**F**) NHE3 protein was virtually undetectable in acutely isolated small intestinal epithelial cells. Kidney tissue from a control (Con) mouse and kidney-specific NHE3 knockout mouse (NHE3^{KS-KO}, [3]) was used to verify antibody specificity. Renal NHE3 protein levels were significantly higher in NHE3^{IEC-KO} compared with control mice. (**G**) Kaplan–Meier survival analysis demonstrates that NHE3^{IEC-KO} mice have decreased survival compared with control mice. Data are expressed as mean ± S.E.M. $n = 4$–6/genotype, except for Kaplan–Meier analysis where n are in parenthesis. Data were analyzed by unpaired Student's t test.

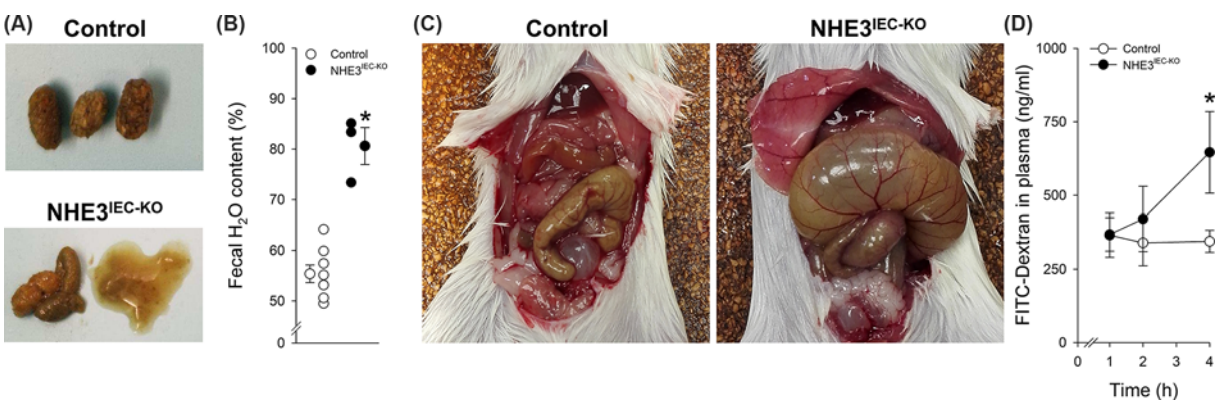

Figure 2. NHE3^{IEC-KO} mice have diarrhea, swollen intestines and increased permeability

(**A**) Representative fecal samples from control and NHE3^{IEC-KO} mice. (**B**) Consistent with watery diarrhea, NHE3^{IEC-KO} mice have higher fecal water content. Of note, ~35% of NHE3^{IEC-KO} mice showed such watery diarrhea that it was not possible to determine water content. (**C**) Representative images of abdominal cavities from control and NHE3^{IEC-KO} mice; the latter showing severe swelling of small intestine, cecum and colon. (**D**) NHE3^{IEC-KO} mice show significantly increased intestinal permeability after 4 h compared with control mice. Data are expressed as mean ± S.E.M.; $n = 4$–8. *$P < 0.05$ versus control. Data were analyzed by unpaired Student's t test.

Clinical Science (2020) **134** 941–953
https://doi.org/10.1042/CS20200065

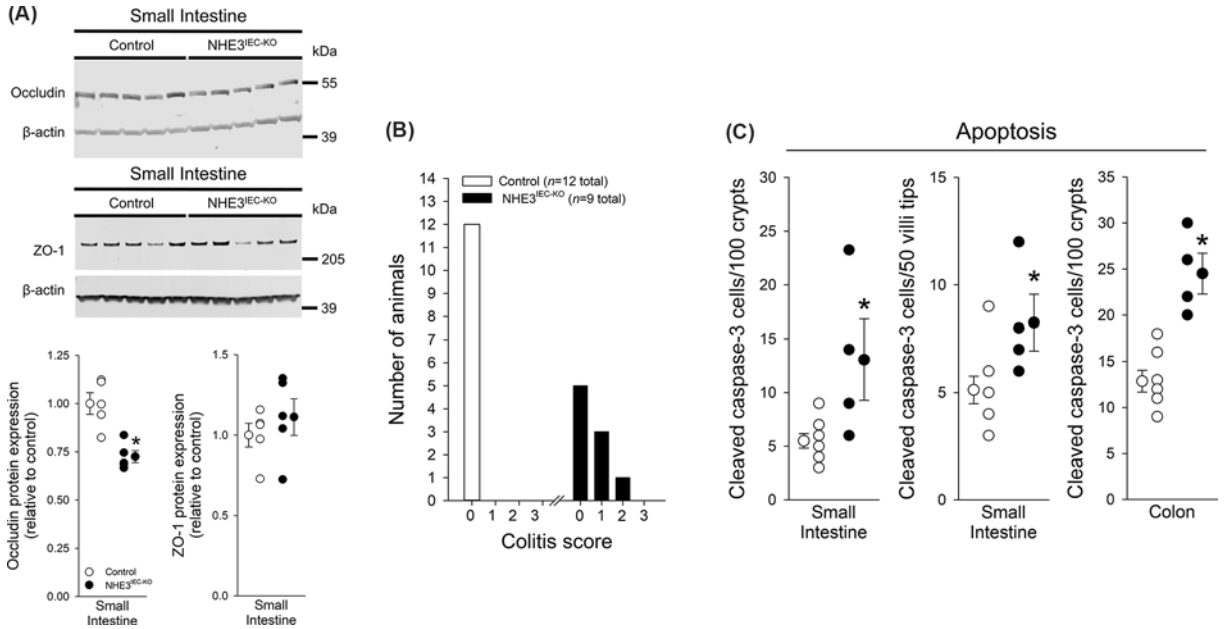

Figure 3. Reduced occludin expression and increased signs of colitis and apoptosis in NHE3^{IEC-KO} mice

(**A**) NHE3^{IEC-KO} mice have reduced occludin expression but unchanged ZO–1 expression. (**B**) Four out of nine NHE3^{IEC-KO} mice show signs of colitis. (**C**) Cleaved caspase-3 staining of small intestinal crypts, villi and colonic crypt indicates increased apoptosis in NHE3^{IEC-KO} mice. Data are expressed as mean ± S.E.M.; $n = 4–12$. *$P < 0.05$ versus control. Data were analyzed by unpaired Student's *t* test.

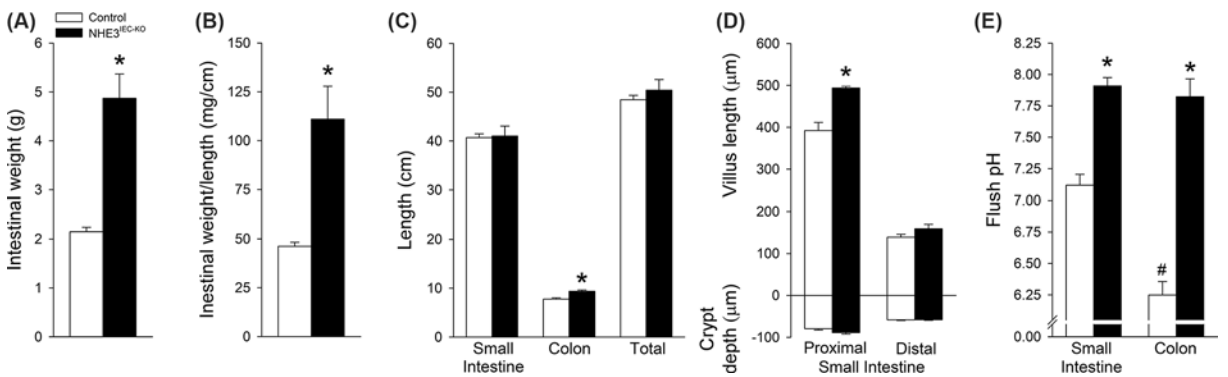

Figure 4. Intestinal contents are more alkaline in NHE3^{IEC-KO} mice

NHE3^{IEC-KO} mice exhibit (**A**) higher intestinal weight and (**B**) weight–to–length ratio compared to control mice. (**C**) Small intestinal length was not changed, but there was a significantly longer colon length in NHE3^{IEC-KO} mice. (**D**) The proximal small intestines of NHE3^{IEC-KO} mice have significantly longer villi compared with control mice. No differences in villi length in distal small intestines or in crypt depth were observed. (**E**) Flush pH of small intestinal and colon contents was significantly more alkaline in NHE3^{IEC-KO} compared with control mice. Data are expressed as mean ± S.E.M.; $n = 4–18$. *$P < 0.05$ versus control. $^{\#}P < 0.05$ versus small intestine control. Data were analyzed by unpaired Student's *t* test or one-way ANOVA followed by Tukey's multiple comparison test.

increased in crypts and villi (∼2.4– and ∼1.6-fold, respectively) of the small intestine in NHE3^{IEC-KO} compared with control mice (Figure 3C), indicating increased apoptosis. In colonic crypts, apoptosis was also increased ∼1.9–fold in NHE3^{IEC-KO} compared with control mice (Figure 3C).

Non-flushed small intestines of NHE3^{IEC-KO} mice were >2-fold heavier compared with control mice (Figure 4A). Similarly, the weight–to–length ratio of the small intestine was ∼2.5–fold higher (Figure 4B), a finding not related to the overall small intestinal length, which was not significantly different between genotypes (Figure 4C). Colons from NHE3^{IEC-KO} mice were ∼1.6 cm longer (∼25%) compared with control mice (Figure 4C) 27 days after tamoxifen

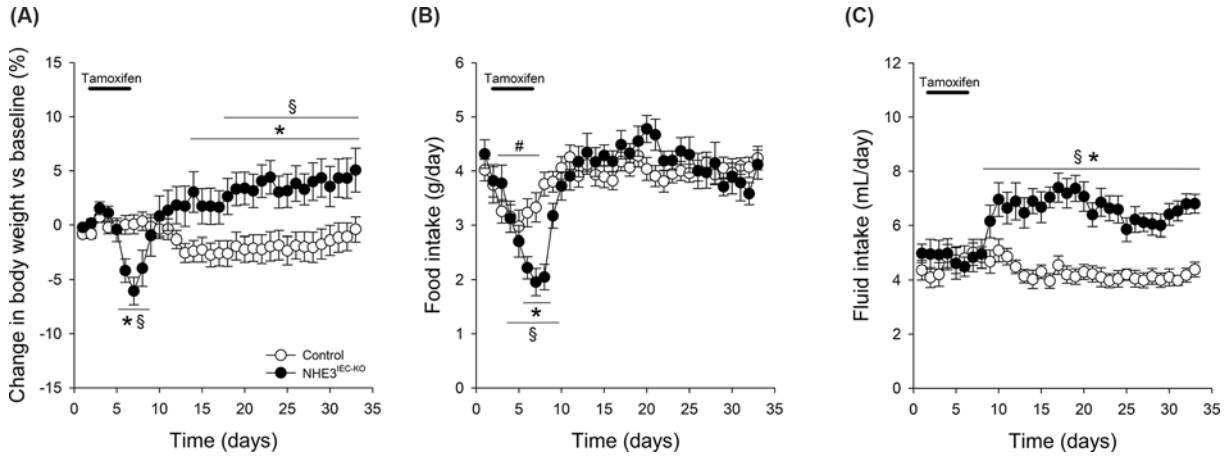

Figure 5. NHE3^{IEC-KO} mice have greater fluid intake and increased body weight

(**A**) NHE3^{IEC-KO} mice show a transient decrease in body weight during tamoxifen administration followed by a significant gain in body weight compared with control mice. (**B**) Tamoxifen administration caused a significant decrease in food intake in both genotypes that was greater in NHE3^{IEC-KO} mice compared with control mice. Subsequently food intake returned to baseline conditions. (**C**) Fluid intake increased after tamoxifen administration in NHE3^{IEC-KO} mice and remained significantly higher compared to control mice. Data are expressed as mean ± S.E.M.; $n = 15$–19. $^{*}P < 0.05$ versus control, $^{\#}P < 0.05$ versus baseline control, $^{\S}P < 0.05$ versus baseline NHE3^{IEC-KO}. Data were analyzed by mixed effects ANOVA followed by two-stage linear step-up procedure of Benjamini, Krieger and Yekutieli.

administration. Villi in proximal small intestine from NHE3^{IEC-KO} mice were ∼100 μm longer compared with control mice (Figure 4D). In contrast, villus length in the distal small intestine, and crypt depth in the proximal and distal small intestine were not significantly different between genotypes (Figure 4D). Colonic flushes from control mice were ∼0.9 pH units lower compared with small intestine (Figure 4E). In contrast, the pH of small intestinal flushes from NHE3^{IEC-KO} mice were ∼0.8 pH units higher than controls and colonic flushes were ∼1.6 pH units higher (Figure 4E). In contrast with controls, no significant differences in flush pH between small intestine and colon were observed in NHE3^{IEC-KO} mice.

Effect of tamoxifen administration on body weight, fluid and food intake in control and NHE3^{IEC-KO} mice

Control ($n = 19$) and NHE3^{IEC-KO} ($n = 15$) mice had no differences in body weight before tamoxifen (baseline) administration (31 ± 1 vs 29 ± 1 g, *NS*). In control mice, body weight did not change during or after tamoxifen administration (Figure 5A). In contrast, NHE3^{IEC-KO} had a significant loss of body weight during initial tamoxifen administration (maximum −6 ± 1% vs baseline), which was followed by a significant increase in body weight compared with baseline (Figure 5A). The immensely fluid-filled cecum and other parts of the intestine (Figure 2C) might have, in conjunction with the increased fluid intake (Figure 5C), contributed to the body weight gain. Food intake was not significantly different between genotypes at baseline (Figure 5B). In control mice, tamoxifen administration caused a transient decrease in food intake (maximum −25%, $P < 0.05$ vs baseline) followed by a return to baseline levels. NHE3^{IEC-KO} mice showed a significantly greater decrease in food intake (maximum −45%, $P < 0.05$ vs baseline) followed by a return to baseline levels (Figure 5B). Fluid intake was not significantly different between genotypes at baseline (Figure 5C) and remained similar in control mice during the remainder of the experimental period. In NHE3^{IEC-KO} mice, 3 days after the end of tamoxifen administration, fluid intake increased significantly compared with baseline and remained elevated for the remainder of the experimental period (Figure 5C). Despite increased fluid intake, relative to controls, NHE3^{IEC-KO} mice had a significantly higher hematocrit (50 ± 2 vs 42 ± 1%, $P < 0.05$) and blood urea nitrogen (BUN) was ∼2.8-fold higher (76 ± 16 vs 27 ± 1, $P < 0.05$), together suggesting dehydration and volume depletion.

Physiological analysis of control and NHE3^{IEC-KO} mice

Baseline blood pH, HCO_3^-, base excess, plasma Na^+, K^+ and aldosterone as well as blood glucose were not significantly different between genotypes (Figure 6A–G). At the end of the experimental period, blood pH (Figure 7A),

Clinical Science (2020) **134** 941–953
https://doi.org/10.1042/CS20200065

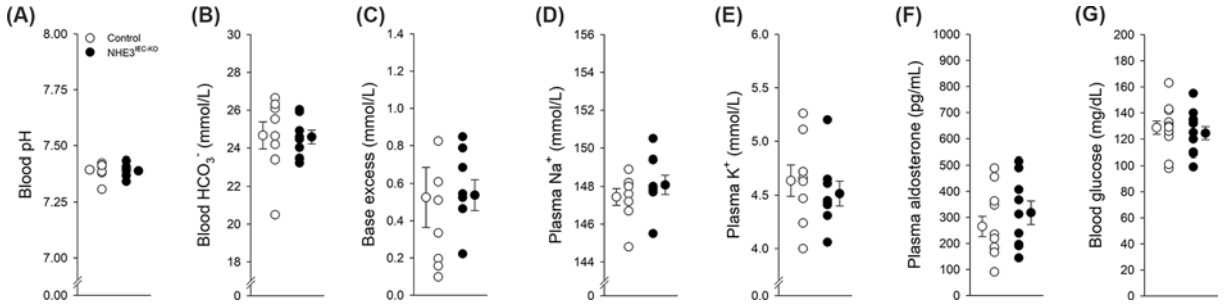

Figure 6. Baseline blood analysis before tamoxifen administration

Before tamoxifen administration no differences between genotypes were observed for (**A**) blood pH, (**B**) blood HCO_3^-, (**C**) base excess, (**D**) Na^+, (**E**) K^+, (**F**) aldosterone or (**G**) glucose. Data are expressed as mean ± S.E.M.; $n = 8$/genotype.

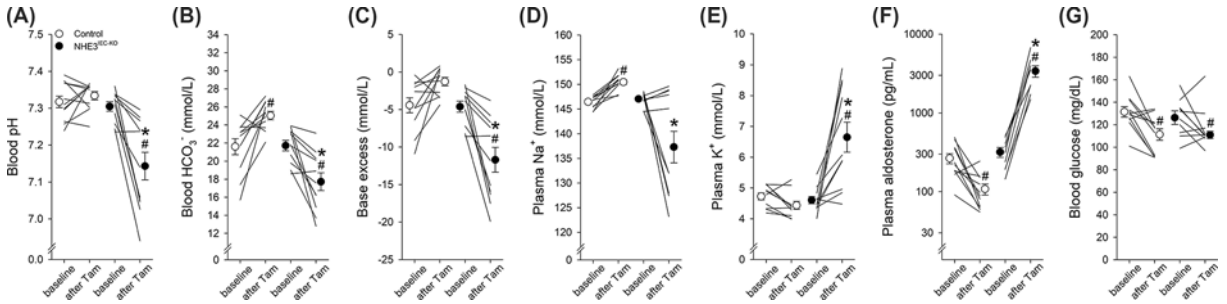

Figure 7. Acid–base and electrolyte disturbances in NHE3$^{IEC\text{-}KO}$ mice after tamoxifen administration

Subsequent to tamoxifen administration, NHE3$^{IEC\text{-}KO}$ mice developed (**A**) lower blood pH, (**B**) lower blood HCO_3^-, (**C**) more negative base excess, (**D**) hyponatremia, (**E**) hyperkalemia and (**F**) hyperaldosteronism. (**G**) Effects on glucose were not different from control mice. Data are expressed as mean ± S.E.M.; $n = 9$–11. Data were analyzed by mixed effects ANOVA followed by Tukey's multiple comparison test.

base excess (Figure 7C) and plasma K^+ (Figure 7E) were not affected in control mice; however, significant increases in blood HCO_3^- (Figure 7B) and plasma Na^+ (Figure 7D) were observed; aldosterone (Figure 7F) and blood glucose (Figure 7G) showed a significant decrease. After tamoxifen administration, blood pH (Δ –0.16 ± 0.04 pH units; Figure 7A), HCO_3^- (Δ –4 ± 1 mmol/L; Figure 7B) and base excess (Δ –7 ± 2 mmol/L; Figure 7C) significantly decreased in NHE3$^{IEC\text{-}KO}$ mice. Consistent with impaired water and Na^+ handling in NHE3$^{IEC\text{-}KO}$ mice, plasma Na^+ decreased (Δ –10 ± 3 mmol/L; Figure 7D). Potentially due to the body's effort to defend against metabolic acidosis in combination with hypovolemia, plasma K^+ significantly increased (Δ 1.9 ± 0.5 mmol/L; Figure 7E). Consistent with an attempt to compensate for hypovolemia and hyponatremia, there were significantly increased plasma aldosterone levels (Δ 3085 ± 551 pg/ml; Figure 7F) in NHE3$^{IEC\text{-}KO}$ mice. The elevated plasma aldosterone levels possibly contributed to a ∼4.6–fold higher ratio of urinary K^+/Na^+ in NHE3$^{IEC\text{-}KO}$ compared to control mice (11.9 ± 2.5 vs 2.6 ± 0.3, $P < 0.05$). Mice with knockout of NHE3 along the renal tubule and collecting duct have a significantly elevated urinary pH and lower urine osmolality [3]. In contrast, urinary pH (5.97 ± 0.1 vs 5.95 ± 0.1, *NS*) and urine osmolality (2133 ± 212 vs 2220 ± 206 mmol/kg, *NS*) were not significantly different between NHE3$^{IEC\text{-}KO}$ mice and control mice.

Discussion

CSD is a disorder with high mortality that is difficult to treat. Determining the role of NHE3 in CSD has been hampered by the lack of a suitable mouse model, with global deletion of NHE3 resulting in very high mortality rates [9,17]. Additionally, prenatal deletion of NHE3 affects intestinal development and epithelial barrier function [26], hampering its usefulness in studies during adulthood. To navigate this problem, we generated tamoxifen–inducible intestinal epithelial cell–specific NHE3 knockout mice (NHE3$^{IEC\text{-}KO}$) by interbreeding NHE3^{loxlox} mice with villin-CreER^{T2} mice. The phenotype of NHE3$^{IEC\text{-}KO}$ mice clearly demonstrates the important homeostatic role of intestinal NHE3. When knockout is induced in adulthood, NHE3$^{IEC\text{-}KO}$ mice have features that

are consistent with patients suffering from CSD: alkaline diarrhea, hyponatremia and metabolic acidosis, alongside activation of the renin–angiotensin–aldosterone system and volume contraction.

$NHE3^{IEC\text{-}KO}$ mice had a complete absence of NHE3 mRNA and protein expression in the small intestine. Although villin is expressed in the mouse kidney [27], NHE3 mRNA expression in kidneys from $NHE3^{IEC\text{-}KO}$ mice was not significantly different from controls. In contrast, renal NHE3 protein expression was significantly greater in $NHE3^{IEC\text{-}KO}$ mice. It is possible that this is a compensatory response. For example metabolic acidosis (which $NHE3^{IEC\text{-}KO}$ mice have, see below) increases renal NHE3 protein expression [28,29] without affecting NHE3 mRNA expression [28]. Why renal NHE3 is not affected remains elusive, but may relate to certain regions of the mouse villin gene being vulnerable to positional effects. The site of chromosomal integration determines transgene expression, which can be altered by neighboring regulatory regions, presumably acting on chromatin conformation. In an unrelated study, we used a non–inducible villin–Cre mouse model and we also did not see differences in renal gene expression between genotypes [30]. We previously attempted to generate constitutive non–inducible intestinal epithelial cell–specific NHE3 knockout mice. This model represented an extreme form of CSD, with only one mouse out of >50 offspring surviving ∼2 weeks and none survived into adulthood [17]. $NHE3^{-/-}$ mice have a 30% survival rate at the age of 30 weeks [9]. $NHE3^{IEC\text{-}KO}$ mice had a ∼27% mortality rate 3 weeks after tamoxifen administration; these mice developed progressive body weight loss and lethargy, requiring them to be euthanized.

$NHE3^{IEC\text{-}KO}$ mice had distended abdomens, fluid-filled intestinal loops and alkaline diarrhea. This is consistent with $NHE3^{-/-}$ mice, which have alkaline diarrhea, increased intestinal weight and increased fluid content [8,31], but importantly $NHE3^{IEC\text{-}KO}$ mice mimic the clinical features of CSD patients [32,33]. The more alkaline pH of the small intestinal and colon contents in $NHE3^{IEC\text{-}KO}$ mice is consistent with reduced H^+ secretion and impaired buffering of secreted HCO_3^-. $NHE3^{-/-}$ mice are more susceptible to mucosal injury [34], with dilated apical junction complexes in the small intestine of $NHE3^{-/-}$ mice [34]. Although this previous observation has, at least in part, been ascribed to developmental effects in $NHE3^{-/-}$ mice, plasma levels of FD–4, a marker of intestinal permeability, is significantly increased 4 h after administration in adult $NHE3^{IEC\text{-}KO}$ mice. Thus, our data are indicative of a continuous important role of NHE3 in the maintenance of epithelial integrity and cell–cell interactions. Our data point toward reduced occludin expression in $NHE3^{IEC\text{-}KO}$ mice contributing to increased intestinal permeability. Reduced occludin expression is a major contributor to increased macromolecule flux across the tight junction barrier of the intestine [35]. In addition, changes in pH, as found in $NHE3^{IEC\text{-}KO}$ mice, were found to affect inter–molecular forces and adhesion strength of tight junction proteins [36]. Additionally, NHE3 is important for intestinal microbial composition and $NHE3^{-/-}$ mice develop spontaneous colitis possibly because of microbial dysbiosis [37–39]. A subset of patients with mutations in NHE3 [16] develop inflammatory bowel disease (IBD). Intestinal epithelial cell apoptosis and loss of barrier function are characteristics of IBD [40,41]; consistent with this, $NHE3^{IEC\text{-}KO}$ mice show increased intestinal apoptosis. Along those lines, our data also indicate that a subset of $NHE3^{IEC\text{-}KO}$ mice develop mild to moderate active colitis. Tenapanor, an orally non–absorbable drug that inhibits NHE3, was just recently approved by the FDA for the treatment of IBD with predominant constipation symptoms [42]. Although the long-term effects of NHE3 inhibition in humans for the course of IBD is unknown, Tenapanor does not appear to cause altered epithelial integrity. This suggests that the altered epithelial integrity in $NHE3^{IEC\text{-}KO}$ and $NHE3^{-/-}$ mice is not due to a lack of Na^+/H^+ exchange, but more a direct role of NHE3 as a scaffolding protein.

Classically, Na^+/H^+ exchange in the proximal tubule of the kidneys is described as the primary determinant of acid–base homeostasis [43]. However, deletion of NHE3 throughout the renal tubule [3,44], or NHE3 knockout in the S1/2 segment of the proximal tubule, does not cause an acid–base phenotype [45]. In contrast, $NHE3^{IEC\text{-}KO}$ mice show a clear metabolic acidosis, lower HCO_3^- levels and lower base excess. Thus, our model unravels the importance of intestinal NHE3 in the regulation of acid–base homeostasis, with the kidney unable to compensate for the magnitude of acid–base disturbance caused by lack of NHE3 in the intestine. Intestinal NHE3 therefore has a physiological role in fending off metabolic acidosis, as emphasized by the significantly increased NHE3 activity and protein in response to NH_4Cl-induced metabolic acidosis [46].

Hyponatremic dehydration is a common finding in children with diarrhea [47], consistent with a role of intestinal NHE3 in transepithelial Na^+ and water absorption [48]. Supporting this role, $NHE3^{IEC\text{-}KO}$ mice show a significantly higher hematocrit and BUN levels, both indirect signs of hypovolemia (we cannot completely exclude a role of reduced glomerular filtration rate to elevate BUN). Subsequent hypovolemic–mediated arginine–vasopressin secretion, coupled to the significantly greater fluid intake to compensate for intestinal fluid loss, is the likely cause of hyponatremia in $NHE3^{IEC\text{-}KO}$ mice. In addition, hypovolemia–mediated increases in ANGII and increased proximal tubule Na^+ reabsorption would limit distal Na^+ delivery, resulting in reduced Na^+/K^+ exchange. This can account for the hyperkalemia in the $NHE3^{IEC\text{-}KO}$ mice, although it is conceivable that the drastic metabolic acidosis contributed to the hyperkalemia. The drastic increase in plasma aldosterone levels in $NHE3^{IEC\text{-}KO}$ mice can be explained by the volume

Clinical Science (2020) **134** 941–953
https://doi.org/10.1042/CS20200065

contraction (activation of renin–angiotensin system) and the hyperkalemia. Hyperkalemia and hyperaldosteronism are common features of patients with CSD [14,33,49].

Another point of discussion from our studies is related to changes in intestinal architecture. In terms of unchanged intestinal but increased colon length, our data from $NHE3^{IEC\text{-}KO}$ mice are consistent with $NHE3^{-/-}$ mice [31]. The latter is possibly a compensatory response to the chronic exposure to an increased volume/electrolyte amount. A similar situation is observed in a mouse model of short bowel syndrome, which develop significantly longer villi and deeper crypts compared with Sham mice [50]. Of note, longer villi were not associated with a better outcome after surgery and could be considered maladaptive. Patients with CSD show mild villus atrophy with hyperplastic crypts [49,51]. In contrast, even though pathophysiological changes were observed in $NHE3^{-/-}$ mice, no histopathological changes in the intestine were described, including no changes in apoptosis [9,34]. Of note, genes involved in apoptosis were significantly up–regulated in $NHE3^{-/-}$ mice [34]. The significantly longer villi in $NHE3^{IEC\text{-}KO}$ mice compared with control mice is indicative of increased mucosal mass. This is supported by a ∼6–fold greater yield of intestinal epithelial cells per unit length of intestinal segment in $NHE3^{-/-}$ mice compared with wild–type mice [34].

In summary, we have generated an inducible intestinal epithelial cell–specific NHE3 knockout mouse model. Studies in these $NHE3^{IEC\text{-}KO}$ mice provide direct *in vivo* evidence that NHE3 has several important homeostatic functions, including but not limited to acid–base regulation, electrolyte balance and water homeostasis. This new mouse model mimics and explains the phenotype of individuals carrying mutations in *SLC9A3*. $NHE3^{IEC\text{-}KO}$ mice are an essential new model to further examine the role of intestinal NHE3 in various physiological and pathophysiological mechanisms.

Clinical perspectives

- The intestine has an important role in acid–base regulation, volume homeostasis and electrolyte transport, some of them directly related to the functional presence of NHE3 in the intestinal mucosa. In patients with mutations in NHE3 congenital sodium diarrhea develops.
- Mice with whole body and constitutive intestinal epithelial cell–specific NHE3 knockout show high mortality rates. We developed a new, tamoxifen–inducible, intestinal epithelial cell–specific NHE3 knockout mouse model that allows for studying the disease in adulthood. The model closely resembles the features seen in patients with congenital sodium diarrhea with a low mortality rate.
- Given that a subset of patients with congenital sodium diarrhea develop inflammatory bowel disease and the recent development of an intestinal–specific NHE3 inhibitor for the treatment of constipation in inflammatory bowel disease and hyperphosphatemia in chronic kidney disease, this new model will help to gain a better understanding of the pathophysiology and pharmacology of NHE3.

Competing Interests

The authors declare that there are no competing interests associated with the manuscript.

Funding

This work was supported by the National Institute of Diabetes and Digestive and Kidney Diseases [grant number 1R01DK110621 (to T.R.)]; American Heart Association Transformational Research Award [grant number 19TPA34850116 (to T.R.)]; the LeDucq Foundation (to R.A.F.); the Danish Medical Research Council; the Novo Nordisk Foundation; American Heart Association predoctoral fellowship [grant number 18PRE33990236 (to J.X.)]; and L.T. by a postdoctoral fellowship [grant number 19POST34400026].

Author Contribution

T.R. designed the work. J.X., L.T., M.T., A.V., R.A.F., J.A.D.R. and T.R. contributed to the acquisition, analysis or interpretation of data for the work. T.R. drafted the work; J.X., L.T., R.A.F. and J.A.D.R. revised it critically for important intellectual content. J.X., L.T., M.T., A.V., R.A.F., J.A.D.R. and T.R. approved the final version of the manuscript.

Abbreviations

CSD, congenital sodium diarrhea; DRA, Cl^-/HCO_3^- exchanger; EDTA, ethylenediaminetetraacetic acid; NHE3, Na^+/H^+ exchanger isoform 3; PBS, phosphate–buffered saline.

References

1 Kato, A. and Romero, M.F. (2011) Regulation of electroneutral NaCl absorption by the small intestine. *Annu. Rev. Physiol.* **73**, 261–281, https://doi.org/10.1146/annurev-physiol-012110-142244
2 Donowitz, M., Mohan, S., Zhu, C.X., Chen, T.E., Lin, R., Cha, B. et al. (2009) NHE3 regulatory complexes. *J. Exp. Biol.* **212**, 1638–1646, https://doi.org/10.1242/jeb.028605
3 Fenton, R.A., Poulsen, S.B., de la Mora Chavez, S., Soleimani, M., Dominguez Rieg, J.A. and Rieg, T. (2017) Renal tubular NHE3 is required in the maintenance of water and sodium chloride homeostasis. *Kidney Int.* **92**, 397–414, https://doi.org/10.1016/j.kint.2017.02.001
4 Wang, J.L., Zhao, L., Zhu, J., Wang, D.K., Ren, M.J., Wang, M. et al. (2019) Expression, Localization, and Effect of High Salt Intake on Electroneutral Na^+/HCO_3^- Cotransporter NBCn2 in Rat Small Intestine: Implication in Intestinal NaCl Absorption. *Front. Physiol.* **10**, 1334, https://doi.org/10.3389/fphys.2019.01334
5 Knickelbein, R., Aronson, P.S., Schron, C.M., Seifter, J. and Dobbins, J.W. (1985) Sodium and chloride transport across rabbit ileal brush border. II. Evidence for Cl^-HCO_3 exchange and mechanism of coupling. *Am. J. Physiol.* **249**, G236–G245
6 Xia, W., Yu, Q., Riederer, B., Singh, A.K., Engelhardt, R., Yeruva, S. et al. (2014) The distinct roles of anion transporters Slc26a3 (DRA) and Slc26a6 (PAT-1) in fluid and electrolyte absorption in the murine small intestine. *Pflugers Arch.* **466**, 1541–1556, https://doi.org/10.1007/s00424-013-1381-2
7 Noonan, W.T., Woo, A.L., Nieman, M.L., Prasad, V., Schultheis, P.J., Shull, G.E. et al. (2005) Blood pressure maintenance in NHE3-deficient mice with transgenic expression of NHE3 in small intestine. *Am. J. Physiol. Regul. Integr. Comp. Physiol.* **288**, R685–R691, https://doi.org/10.1152/ajpregu.00209.2004
8 Schultheis, P.J., Clarke, L.L., Meneton, P., Miller, M.L., Soleimani, M., Gawenis, L.R. et al. (1998) Renal and intestinal absorptive defects in mice lacking the NHE3 Na^+/H^+ exchanger. *Nat. Genet.* **19**, 282–285, https://doi.org/10.1038/969
9 Bradford, E.M., Sartor, M.A., Gawenis, L.R., Clarke, L.L. and Shull, G.E. (2009) Reduced NHE3-mediated Na+ absorption increases survival and decreases the incidence of intestinal obstructions in cystic fibrosis mice. *Am. J. Physiol. Gastrointest. Liver Physiol.* **296**, G886–G898, https://doi.org/10.1152/ajpgi.90520.2008
10 Ledoussal, C., Lorenz, J.N., Nieman, M.L., Soleimani, M., Schultheis, P.J. and Shull, G.E. (2001) Renal salt wasting in mice lacking NHE3 Na+/H+ exchanger but not in mice lacking NHE2. *Am. J. Physiol. Renal. Physiol.* **281**, F718–F727, https://doi.org/10.1152/ajprenal.2001.281.4.F718
11 Woo, A.L., Noonan, W.T., Schultheis, P.J., Neumann, J.C., Manning, P.A., Lorenz, J.N. et al. (2003) Renal function in NHE3-deficient mice with transgenic rescue of small intestinal absorptive defect. *Am. J. Physiol. Renal. Physiol.* **284**, F1190–F1198, https://doi.org/10.1152/ajprenal.00418.2002
12 Holmberg, C. and Perheentupa, J. (1985) Congenital Na^+ diarrhea: a new type of secretory diarrhea. *J. Pediatr.* **106**, 56–61, https://doi.org/10.1016/S0022-3476(85)80465-0
13 Booth, I.W., Stange, G., Murer, H., Fenton, T.R. and Milla, P.J. (1985) Defective jejunal brush-border Na^+/H^+ exchange: a cause of congenital secretory diarrhoea. *Lancet* **1**, 1066–1069, https://doi.org/10.1016/S0140-6736(85)92369-4
14 Janecke, A.R., Heinz-Erian, P., Yin, J., Petersen, B.S., Franke, A., Lechner, S. et al. (2015) Reduced sodium/proton exchanger NHE3 activity causes congenital sodium diarrhea. *Hum. Mol. Genet.* **24**, 6614–6623, https://doi.org/10.1093/hmg/ddv367
15 Gurney, M.A., Laubitz, D., Ghishan, F.K. and Kiela, P.R. (2017) Pathophysiology of Intestinal Na^+/H^+ exchange. *Cell Mol. Gastroenterol. Hepatol.* **3**, 27–40, https://doi.org/10.1016/j.jcmgh.2016.09.010
16 Janecke, A.R., Heinz-Erian, P. and Muller, T. (2016) Congenital Sodium Diarrhea: A Form of Intractable Diarrhea, With a Link to Inflammatory Bowel Disease. *J. Pediatr. Gastroenterol. Nutr.* **63**, 170–176, https://doi.org/10.1097/MPG.0000000000001139
17 Dominguez Rieg, J.A., de la Mora Chavez, S. and Rieg, T. (2016) Novel developments in differentiating the role of renal and intestinal sodium hydrogen exchanger 3. *Am. J. Physiol. Regul. Integr. Comp. Physiol.* **311**, R1186–R1191, https://doi.org/10.1152/ajpregu.00372.2016
18 Li, H.C., Du, Z., Barone, S., Rubera, I., McDonough, A.A., Tauc, M. et al. (2013) Proximal tubule specific knockout of the Na^+/H^+ exchanger NHE3: effects on bicarbonate absorption and ammonium excretion. *J. Mol. Med. (Berl)* **91**, 951–963, https://doi.org/10.1007/s00109-013-1015-3
19 Dominguez, J.A., Xie, Y., Dunne, W.M., Yoseph, B.P., Burd, E.M., Coopersmith, C.M. et al. (2012) Intestine-specific Mttp deletion decreases mortality and prevents sepsis-induced intestinal injury in a murine model of Pseudomonas aeruginosa pneumonia. *PLoS ONE* **7**, e49159, https://doi.org/10.1371/journal.pone.0049159
20 Poulsen, S.B., Kristensen, T.B., Brooks, H.L., Kohan, D.E., Rieg, T. and Fenton, R.A. (2017) Role of adenylyl cyclase 6 in the development of lithium-induced nephrogenic diabetes insipidus. *JCI Insight* **2**, e91042, https://doi.org/10.1172/jci.insight.91042
21 Thomas, L., Xue, J., Murali, S.K., Fenton, R.A., Dominguez Rieg, J.A. and Rieg, T. (2019) Pharmacological Npt2a Inhibition Causes Phosphaturia and Reduces Plasma Phosphate in Mice with Normal and Reduced Kidney Function. *J. Am. Soc. Nephrol.* **30**, 2128–2139, https://doi.org/10.1681/ASN.2018121250
22 Dominguez, J.A., Samocha, A.J., Liang, Z., Burd, E.M., Farris, A.B. and Coopersmith, C.M. (2013) Inhibition of IKKbeta in enterocytes exacerbates sepsis-induced intestinal injury and worsens mortality. *Crit. Care Med.* **41**, e275–e285, https://doi.org/10.1097/CCM.0b013e31828a44ed
23 Fenton, R.A., Murali, S.K., Kaji, I., Akiba, Y., Kaunitz, J.D., Kristensen, T.B. et al. (2019) Adenylyl Cyclase 6 Expression Is Essential for Cholera Toxin-Induced Diarrhea. *J. Infect. Dis.* **220**, 1719–1728, https://doi.org/10.1093/infdis/jiz013
24 Dominguez Rieg, J.A., Chirasani, V.R., Koepsell, H., Senapati, S., Mahata, S.K. and Rieg, T. (2016) Regulation of intestinal SGLT1 by catestatin in hyperleptinemic type 2 diabetic mice. *Lab. Invest.* **96**, 98–111, https://doi.org/10.1038/labinvest.2015.129

Clinical Science (2020) **134** 941–953
https://doi.org/10.1042/CS20200065

25 Rieg, T., Pothula, K., Schroth, J., Satriano, J., Osswald, H., Schnermann, J. et al. (2008) Vasopressin regulation of inner medullary collecting ducts and compensatory changes in mice lacking adenosine A_1 receptors. *Am. J. Physiol. Renal. Physiol.* **294**, F638–F644, https://doi.org/10.1152/ajprenal.00344.2007
26 Odenwald, M.A. and Turner, J.R. (2017) The intestinal epithelial barrier: a therapeutic target? *Nat. Rev. Gastroenterol. Hepatol.* **14**, 9–21, https://doi.org/10.1038/nrgastro.2016.169
27 Ongeri, E.M., Anyanwu, O., Reeves, W.B. and Bond, J.S. (2011) Villin and actin in the mouse kidney brush-border membrane bind to and are degraded by meprins, an interaction that contributes to injury in ischemia-reperfusion. *Am. J. Physiol. Renal. Physiol.* **301**, F871–F882, https://doi.org/10.1152/ajprenal.00703.2010
28 Ambuhl, P.M., Amemiya, M., Danczkay, M., Lotscher, M., Kaissling, B., Moe, O.W. et al. (1996) Chronic metabolic acidosis increases NHE3 protein abundance in rat kidney. *Am. J. Physiol.* **271**, F917–F925
29 Wu, M.S., Biemesderfer, D., Giebisch, G. and Aronson, P.S. (1996) Role of NHE3 in mediating renal brush border Na^+-H^+ exchange. Adaptation to Metabolic acidosis. *J. Biol. Chem.* **271**, 32749–32752
30 Fenton, R.A., Murali, S.K., Kaji, I., Akiba, Y., Kaunitz, J.D., Kristensen, T.B. et al. (2019) Adenylyl cyclase 6 expression is essential for cholera toxin-induced diarrhea. *J. Infect. Dis.*, https://doi.org/10.1093/infdis/jiz013
31 Ledoussal, C., Woo, A.L., Miller, M.L. and Shull, G.E. (2001) Loss of the NHE2 Na^+/H^+ exchanger has no apparent effect on diarrheal state of NHE3-deficient mice. *Am. J. Physiol. Gastrointest. Liver Physiol.* **281**, G1385–G1396, https://doi.org/10.1152/ajpgi.2001.281.6.G1385
32 Thiagarajah, J.R., Kamin, D.S., Acra, S., Goldsmith, J.D., Roland, J.T., Lencer, W.I. et al. (2018) Advances in Evaluation of Chronic Diarrhea in Infants. *Gastroenterology* **154**, 2045e2046–2059e2046, https://doi.org/10.1053/j.gastro.2018.03.067
33 Kidowaki, T., Funaki, H., Mizuta, R., Nishiki, T. and Takada, H. (1993) Treatment of an infant with congenital sodium diarrhea by oral rehydration. *Acta Paediatr. Jpn.* **35**, 49–52, https://doi.org/10.1111/j.1442-200X.1993.tb03005.x
34 Kiela, P.R., Laubitz, D., Larmonier, C.B., Midura-Kiela, M.T., Lipko, M.A., Janikashvili, N. et al. (2009) Changes in mucosal homeostasis predispose NHE3 knockout mice to increased susceptibility to DSS-induced epithelial injury. *Gastroenterology* **137**, 965-975, 975e961-e910, https://doi.org/10.1053/j.gastro.2009.05.043
35 Al-Sadi, R., Khatib, K., Guo, S., Ye, D., Youssef, M. and Ma, T. (2011) Occludin regulates macromolecule flux across the intestinal epithelial tight junction barrier. *Am. J. Physiol. Gastrointest. Liver Physiol.* **300**, G1054–G1064, https://doi.org/10.1152/ajpgi.00055.2011
36 Lim, T.S., Vedula, S.R., Hui, S., Kausalya, P.J., Hunziker, W. and Lim, C.T. (2008) Probing effects of pH change on dynamic response of Claudin-2 mediated adhesion using single molecule force spectroscopy. *Exp. Cell Res.* **314**, 2643–2651, https://doi.org/10.1016/j.yexcr.2008.05.015
37 Harrison, C.A., Laubitz, D., Ohland, C.L., Midura-Kiela, M.T., Patil, K., Besselsen, D.G. et al. (2018) Microbial dysbiosis associated with impaired intestinal Na^+/H^+ exchange accelerates and exacerbates colitis in ex-germ free mice. *Mucosal Immunol.* **11**, 1329–1341, https://doi.org/10.1038/s41385-018-0035-2
38 Larmonier, C.B., Laubitz, D., Hill, F.M., Shehab, K.W., Lipinski, L., Midura-Kiela, M.T. et al. (2013) Reduced colonic microbial diversity is associated with colitis in NHE3-deficient mice. *Am. J. Physiol. Gastrointest. Liver Physiol.* **305**, G667–G677, https://doi.org/10.1152/ajpgi.00189.2013
39 Engevik, M.A., Aihara, E., Montrose, M.H., Shull, G.E., Hassett, D.J. and Worrell, R.T. (2013) Loss of NHE3 alters gut microbiota composition and influences Bacteroides thetaiotaomicron growth. *Am. J. Physiol. Gastrointest. Liver Physiol.* **305**, G697–G711, https://doi.org/10.1152/ajpgi.00184.2013
40 Blander, J.M. (2018) On cell death in the intestinal epithelium and its impact on gut homeostasis. *Curr. Opin. Gastroenterol.* **34**, 413–419, https://doi.org/10.1097/MOG.0000000000000481
41 Gunther, C., Neumann, H., Neurath, M.F. and Becker, C. (2013) Apoptosis, necrosis and necroptosis: cell death regulation in the intestinal epithelium. *Gut* **62**, 1062–1071, https://doi.org/10.1136/gutjnl-2011-301364
42 Markham, A. (2019) Tenapanor: First Approval. *Drugs* **79**, 1897–1903, https://doi.org/10.1007/s40265-019-01215-9
43 Bobulescu, I.A. and Moe, O.W. (2009) Luminal Na^+/H^+ exchange in the proximal tubule. *Pflugers Arch.* **458**, 5–21, https://doi.org/10.1007/s00424-008-0595-1
44 Onishi, A., Fu, Y., Darshi, M., Crespo-Masip, M., Huang, W., Song, P. et al. (2019) Effect of renal tubule-specific knockdown of the Na^+/H^+ exchanger NHE3 in Akita diabetic mice. *Am. J. Physiol. Renal. Physiol.* **317**, F419–F434, https://doi.org/10.1152/ajprenal.00497.2018
45 Li, X.C., Soleimani, M., Zhu, D., Rubera, I., Tauc, M., Zheng, X. et al. (2018) Proximal Tubule-Specific Deletion of the NHE3 (Na^+/H^+ Exchanger 3) Promotes the Pressure-Natriuresis Response and Lowers Blood Pressure in Mice. *Hypertension* **72**, 1328–1336, https://doi.org/10.1161/HYPERTENSIONAHA.118.10884
46 Lucioni, A., Womack, C., Musch, M.W., Rocha, F.L., Bookstein, C. and Chang, E.B. (2002) Metabolic acidosis in rats increases intestinal NHE2 and NHE3 expression and function. *Am. J. Physiol. Gastrointest. Liver Physiol.* **283**, G51–G56, https://doi.org/10.1152/ajpgi.00529.2001
47 Caksen, H., Odabas, D., Sar, S., Celebi, V., Arslan, S., Kuru, M. et al. (2001) Hyponatremic dehydration: an analysis of 78 cases. *Int. Urol. Nephrol.* **33**, 445–448, https://doi.org/10.1023/A:1019563222488
48 Clarke, L.L. and Harline, M.C. (1996) CFTR is required for cAMP inhibition of intestinal Na^+ absorption in a cystic fibrosis mouse model. *Am. J. Physiol.* **270**, G259–G267
49 Muller, T., Wijmenga, C., Phillips, A.D., Janecke, A., Houwen, R.H., Fischer, H. et al. (2000) Congenital sodium diarrhea is an autosomal recessive disorder of sodium/proton exchange but unrelated to known candidate genes. *Gastroenterology* **119**, 1506–1513, https://doi.org/10.1053/gast.2000.20514
50 Berlin, P., Reiner, J., Wobar, J., Bannert, K., Glass, A., Walter, M. et al. (2019) Villus Growth, Increased Intestinal Epithelial Sodium Selectivity, and Hyperaldosteronism Are Mechanisms of Adaptation in a Murine Model of Short Bowel Syndrome. *Dig. Dis. Sci.* **64**, 1158–1170, https://doi.org/10.1007/s10620-018-5420-x

51 Keller, K.M., Wirth, S., Baumann, W., Sule, D. and Booth, I.W. (1990) Defective jejunal brush border membrane sodium/proton exchange in association with lethal familial protracted diarrhoea. *Gut* **31**, 1156–1158, https://doi.org/10.1136/gut.31.10.1156

(A) NHE3^{IEC-KO}
Normal colon mucosa, score 0

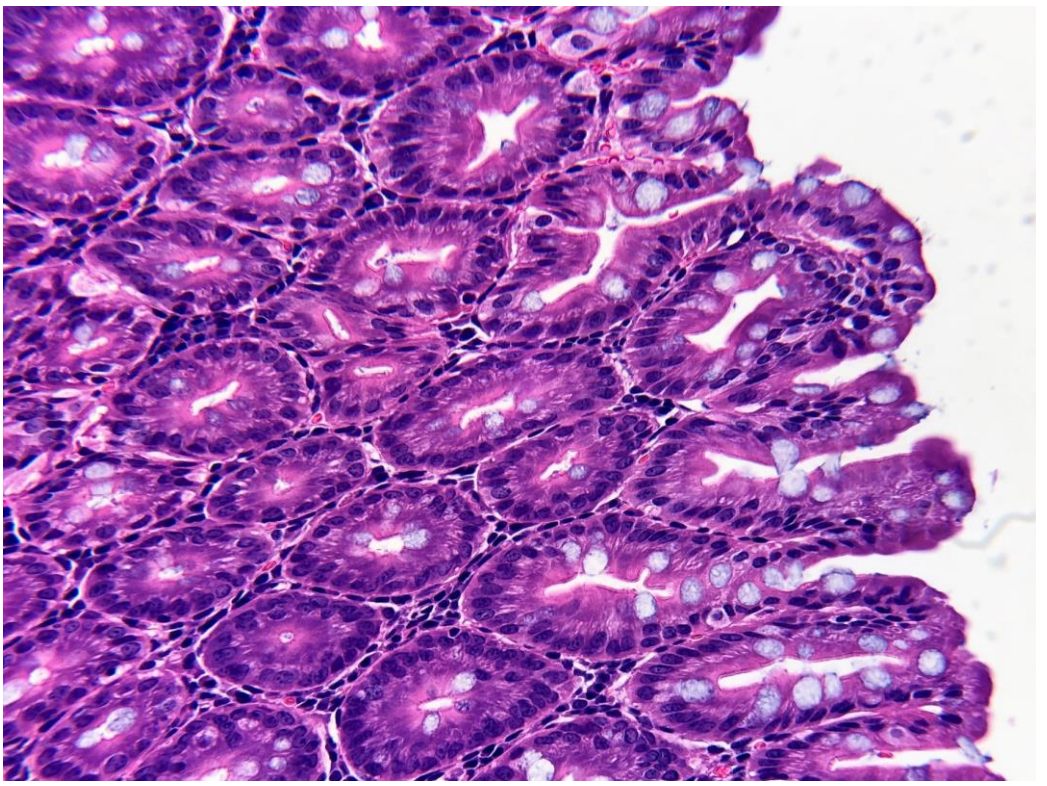

(B) NHE3^{IEC-KO}
Abnormal colon mucosa, colitis score 1

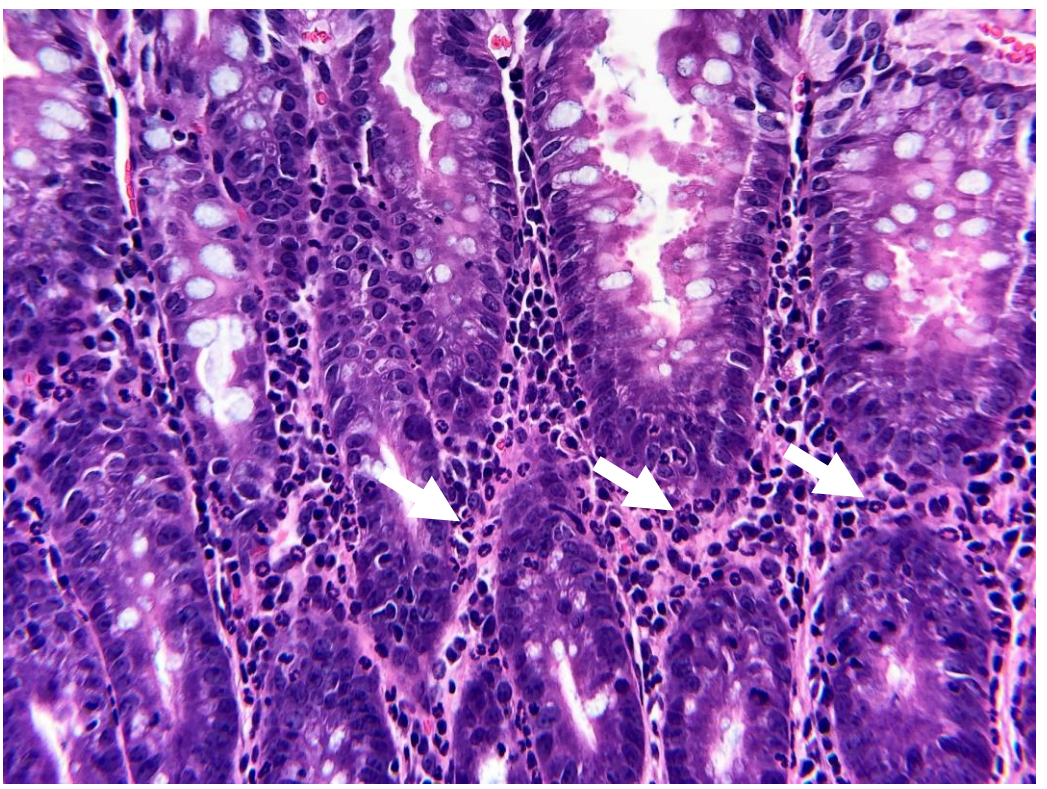

(C) NHE3^{IEC-KO}
Abnormal colon mucosa, colitis score 2

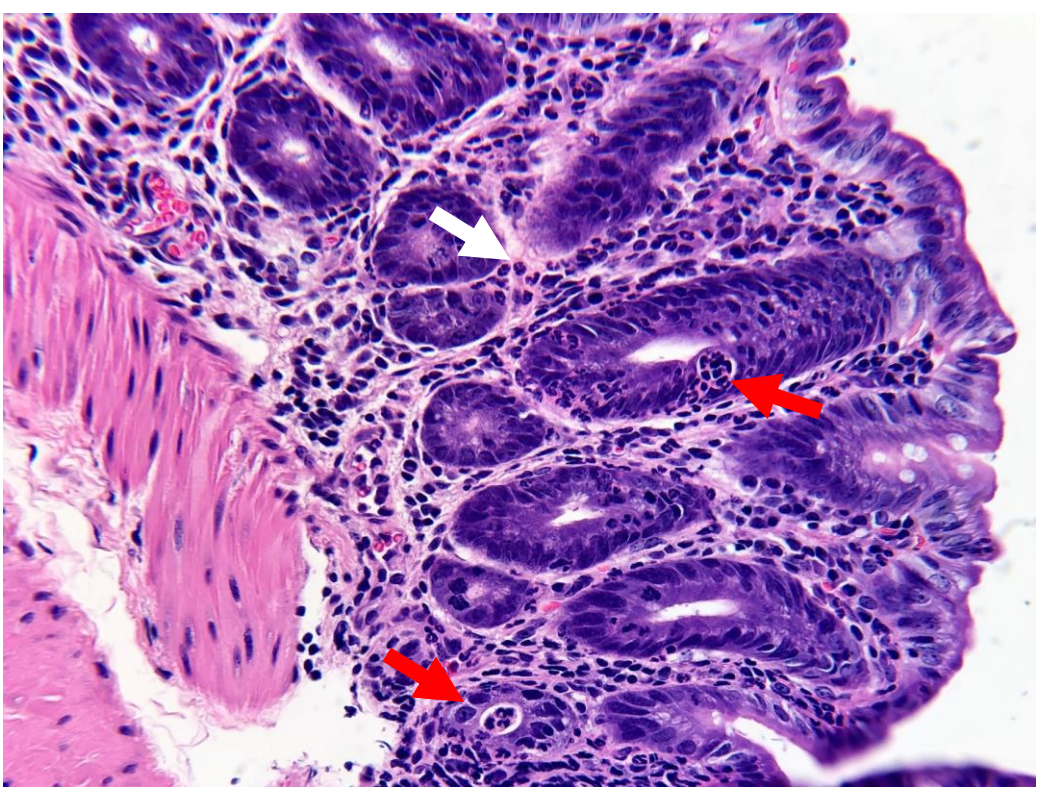

Supplementary Figure S1

Supplementary Figure S1. Histopathology of colon mucosa in NHE3^{IEC-KO} mice

(A) Normal colon mucosa of NHE3^{IEC-KO} mice. (B) Abnormal colon mucosa in NHE3^{IEC-KO} mice showing mild inflammation with cryptitis. White arrows indicate neutrophils in lamina propria and in the crypt epithelial cells (cryptitis). (C) Abnormal colon mucosa in NHE3^{IEC-KO} showing moderate inflammation with cryptitis and crypt abscess. White arrows indicate neutrophils and red arrows indicate cryptitis and crypt abscess.